Photodissociation Imaging of Diatomic Sulfur (S_2)†

Pim W. J. M. Frederix, Chung-Hsin Yang, Gerrit C. Groenenboom, and David H. Parker*

Institute for Molecules and Materials, Radboud University Nijmegen, Heyendaalseweg 135, 6525 AJ Nijmegen, The Netherlands

Koutayba Alnama

Laboratoire de Photophysique Moléculaire, Université de Paris-Sud, 91405 ORSAY CEDEX, France

Colin M. Western and Andrew J. Orr-Ewing

School of Chemistry, University of Bristol, Cantock's Close, Bristol BS8 1TS, United Kingdom

Received: May 31, 2009; Revised Manuscript Received: July 29, 2009

The photodissociation of diatomic sulfur, S_2, in the region of the first dissociation limit is studied with velocity map imaging. Correlated fine structure distributions $P(J1,J2)$ for the two $S(^3P_J)$ fragments are determined at selected photolysis wavelengths. Image analysis of the speed distributions of the atomic fragments following product-state-specific detection results in a revision of the bond energy to $D_0 = 35636.9 \pm 2.5$ cm^{-1} with respect to the lowest rovibrational level. This value arises from reinterpretation of previous spectroscopic data showing onset of predissociation in the $B^3\Sigma_u^-$ state, as the measurements presented here demonstrate that the long-range correlation of the excited state invoked as causing the dissociation is $S(^3P_2) + S(^3P_2)$ rather than $S(^3P_2) + S(^3P_1)$. The wavelength dependence of data for the $S(^3P_2) + S(^3P_2)$ channel suggests involvement of photoexcitation through the optically forbidden Herzberg continuum bands in addition to dissociation initiated via the optically allowed $B^3\Sigma_u^- - X^3\Sigma_g^-$ and $B''^3\Pi_u - X^3\Sigma_g^-$ bands. Changes in product recoil velocity angular distributions and atomic angular momentum polarization were also measured as a function of dissociation wavelength. The results are compared with predictions from an adiabatic model for dissociation, which provides a basis for interpretation but does not explain quantitatively the experimental results.

Introduction

Diatomic sulfur is an important intermediate in combustion processes of sulfur-containing molecules and in the chemistry of planetary atmospheres; for example, it arises from volcanic activity,[1] and emission from S_2 was observed in Jupiter's atmosphere after the impact of the Shoemaker-Levy 9 comet.[2] Spectroscopic signatures of S_2 have also been observed from cometary atmospheres[3−5] and dense molecular clouds.[6,7]

As a homonuclear diatomic molecule, S_2 photoexcitation and photoemission are limited by symmetry selection rules to electronic transitions occurring in the visible to ultraviolet (UV) region of the spectrum. In spite of its low chemical stability under standard conditions, the presence of S_2 can be monitored by emission arising from the optically allowed $B^3\Sigma_u^- - X^3\Sigma_g^-$ transition, which corresponds to the Schumann−Runge transition of the isovalent O_2 molecule. This B−X emission band spans wavelengths in the UV and visible regions ranging from 250 to 700 nm. The ultraviolet absorption spectrum of S_2 shows an onset of predissociation at wavelengths shorter than ∼281 nm, which marks the upper energy limit of the first ($S(^3P) + S(^3P)$) dissociation channel. From this onset, and knowledge of the spectroscopy, the bond dissociation energy D_0 can, in principle, be determined.

Potential energy curves derived from electronic structure calculations by Wheeler et al.[15] for the lower-lying electronic states of S_2 are shown in Figure 1. At large interatomic distances, the $B^3\Sigma_u^-$ state correlates diabatically to the second dissociation channel ($S(^3P) + S(^1D)$), which lies at an energy $\Delta E = 9238.61$ cm^{-1} (corresponding to the $S(^1D) - S(^3P)$ term difference) above the lowest dissociation limit. The $B^3\Sigma_u^-$ state is, however, predissociated (for $v' \geq 10$) by interaction with some or all of the ungerade states that correlate asymptotically with the first

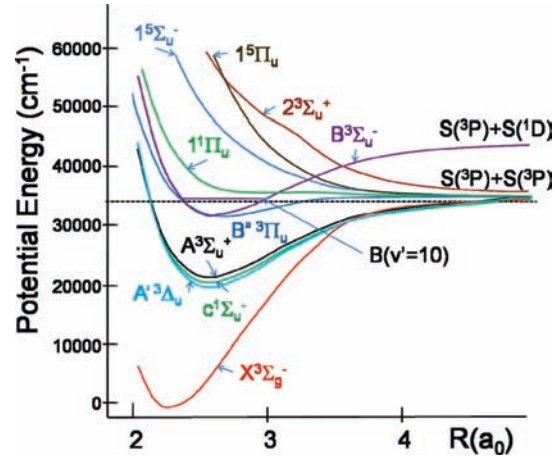

Figure 1. Potential energy curves for the ground and low-lying excited ungerade electronic states of S_2 showing correlations to the first and second dissociation channels. The PE curves are based on electronic structure calculations by Wheeler et al.[15] that did not include the effects of spin−orbit coupling.

† Part of the "Vincenzo Aquilanti Festschrift".

* Author for correspondence. E-mail: parker@science.ru.nl.

10.1021/jp905104u
Published on Web 09/15/2009

dissociation limit. This includes several repulsive curves ($1^1\Pi_u$, $1^5\Sigma_u^-$, $1^5\Pi_u$, and $2^3\Sigma_u^+$) and the bound $B''^3\Pi_u$, $A^3\Sigma_u^+$, $A'^3\Delta_u$, and $c^1\Sigma_u^-$ states.

In previous studies[15] of S_2 photoexcitation, line broadening in the absorption spectrum, which is a signature of reduction in excited state lifetime caused by the onset of dissociation pathways, was used to deduce which PE curve(s) cause the predissociation of the $B^3\Sigma_u^-$ state. Such studies did not, however, provide information on the subsequent dissociation dynamics, and any predictions about the production of different fine-structure (J) states of the resultant $S(^3P_J)$ atoms could only be based on limiting case models of adiabatic or sudden dissociation. Analysis of the rovibrational structure of the lower vibrational levels of the B state is complicated by perturbations, especially resulting from interactions with the bound $B''^3\Pi_u$ state.[8] Many efforts have been made to perform deperturbation analyses, with the early work summarized by Barrow and Du Parcq.[9] Only after the supersonic free jet studies of Matsumi et al.,[10,11] in which transitions to the B and B″ states were distinguished, was a full assignment of the band system possible. The system was theoretically studied by Pradhan and Partridge[12] in 1996, and a complete deperturbation analysis was subsequently performed by Green and Western.[13,14]

As a consequence of the strongly overlapping B and B″ states, an accurate measure of the bond energy of S_2 remained elusive until 1968. Berkowitz and Chupka reported a value of 35326 $\pm$ 70 cm^{-1} from their photoionization study,[16] and around the same time, Ricks and Barrow determined the limit by comparing the absorption and emission spectra of sulfur vapor to determine the onset of predissociation.[17] They identified the last emitting level and the first predissociated level for a variety of vibrational levels and spin components for the B state of $^{32}S_2$, $^{32}S^{34}S$, and $^{34}S_2$. Extrapolating to $J = 0$ indicated that all three spin components had the same dissociation limit, specifically 35999.0 cm^{-1} above the ground state minimum. Given that all three components of the B state were affected by predissociation, Ricks and Barrow assigned a 1_u state as the predissociating state and concluded that the products of this channel must be $S(^3P_2)$ + $S(^3P_1)$ (hereafter referred to as (2,1)), based upon correlation arguments. Combining this limit with the known $S(^3P_2)$ and $S(^3P_1)$ fine structure separation, 396.055 cm^{-1}, and the $^{32}S_2$ zero-point energy (362.123 cm^{-1}) gives a D_0 value of 35240.8 $\pm$ 2.5 cm^{-1}. Note that the value quoted by Ricks and Barrow is 35216.4 $\pm$ 2.5 cm^{-1}, which corresponds to the dissociation energy with respect to the zero of the rotational energy level expression they used for the ground state. Given the relatively large spin−spin interaction in the ground state ($\lambda = 11.7761$ cm^{-1}), the lowest rotational level ($J = 0$, $N = 1$) is actually significantly ($\sim 2\lambda$) below this.

This value for D_0 has remained generally accepted, and was supported by the subsequent deperturbation analysis of laser induced fluorescence (LIF) spectra of S_2 B/B″−X band systems in a molecular beam by Green and Western.[13,14] A detailed examination of the region around the dissociation limit found a cutoff in fluorescence in two of the highest vibrational levels of the B″ state at an energy consistent with the earlier D_0 value.[14] Levels with short fluorescence lifetimes were, however, observed above this dissociation threshold, including two that were assigned to the B″ state. Such an assignment is only possible if the B″ state correlates to a dissociation limit higher than the (2,1) asymptote expected from application of the noncrossing rule for states of the same symmetry. This, and further spectroscopic evidence, led Green and Western to propose correlation of the $\Omega = 0^+$, 1, and 2 components of the B″ state to the $^3P_2 + {}^3P_0$ (i.e., (2,0)) dissociation limit. The later study by Wheeler et al.[15] investigated the levels of the B state above the first dissociation limit, measuring linewidths for $v' = 10-19$ in the range 1 to >20 cm^{-1} by cavity ring down spectroscopy (CRDS). The experimental linewidths were used to derive excited state lifetimes, and interpretation of the data was supplemented by modeling of the predissociation rates, aided by *ab initio* calculation of potential energy curves of *u* symmetry correlating to the $S(^3P) + S(^3P)$ dissociation limit. The combination of experimental measurements and calculated lifetimes implicated the $1^1\Pi_u$ state in the predissociation of the B state for $v' \leq 16$, with higher-lying repulsive states becoming important for predissociation of the $v' \geq 17$ levels.

In the present work, the photodissociation of S_2 is studied by direct detection of the $S(^3P_J)$ products using the velocity map imaging (VMI) technique.[18] The opportunity that VMI offers to specify the observed photoproduct channel has led to several surprising results regarding the total kinetic energy release (TKER) of the nascent atoms. Most notably, we present a revised value of the bond dissociation energy that is unambiguously derived from the TKER data. Furthermore, with VMI, the angular anisotropy of photofragment recoil velocities and electronic angular momentum alignment of the nascent $S(^3P_J)$ atoms can be determined, providing insights into the dynamics of bond scission. Van Brunt and Zare[19] first drew relations between atomic angular momentum polarization and photodissociation pathways based on the correlation rules derived by Wigner and Witmer,[20] among others. Recently, Clark et al.[21] and Suits and Vasyutinski[22] reviewed the study of atomic angular momentum polarization resulting from photodissociation of diatomic molecules. The use of linearly polarized light can induce alignment and, under some circumstances, orientation of the angular momentum in the photofragments. Experimental determination of these effects, whether expressed as a set of orientation and alignment parameters or as population distributions of m_J angular momentum projection sublevels, provides a sensitive probe for nonadiabaticity in the dissociation dynamics.

A comparison of the photodynamics of S_2 with those of the isovalent O_2 molecule is instructive because a large body of information exists on the photodissociation dynamics of molecular oxygen.[23] There are several significant differences in the electronic structure of the two molecules that concern the $A^3\Sigma_u^+$,[24] $c^1\Sigma_u^+$,[25] and $A'^3\Delta_u$ [26] states (the upper states of the Herzberg bands) which are more strongly bound in S_2 than in O_2. In addition, the upper level of the well-known Schumann−Runge bands, the $B^3\Sigma_u^-$ state, is lower in energy in S_2, with bound levels lying below the first dissociation limit. In O_2, the $1^3\Pi_u$ state, which is equivalent to the S_2 $B''^3\Pi_u$ state, lies at energies above the first dissociation limit and is repulsive in character. Likewise, the $1^1\Pi_u$ state of O_2 is repulsive but becomes very weakly bound in S_2.

In O_2, photodissociation takes place at wavelengths shorter than 242 nm through the electric-dipole forbidden Herzberg continuum. Electric-dipole allowed electronic transitions to bound states are only observed at wavelengths below 200 nm, at which energies the B state is reached. The B state vibrational levels undergo predissociation to the first dissociation limit.[27,28] In S_2, the B state levels extend below the first dissociation limit, and electric-dipole allowed transitions to these dominate the absorption spectrum. These bound levels of the B state are mixed with levels of the B″ state, but as we show in this study, photoexcitation of B/B″ levels of S_2 above the dissociation limit does not appear to dominate the dissociation process, although the levels are known to be excited in absorption and predisso-

ciative in character. In addition, absorption to a continuum, possibly the Herzberg continuum of S_2, allows competitive but direct access to the lowest dissociation channel.

Experimental Section

The velocity map imaging setup used in this study has been described in detail elsewhere.[18] A pulsed supersonic molecular beam created by a Jordan valve directed parallel to the time-of-flight (TOF) axis first passed through a small discharge ring and a skimmer mounted 15 mm downstream from the nozzle and entered the imaging region between two open electrode plates another 200 mm downstream, where photoexcitation took place. The S_2 molecules formed in the discharge were dissociated and ionized by UV light from two independent tunable dye lasers with nanosecond pulse lengths. Permanent positive voltages were applied on the electrode plates, with their ratio set for velocity focusing, whereby all ions with the same initial velocity vector were projected on the same position on a two-dimensional (2-D) microchannel plate (MCP) detector, independent of the position of formation, after flying through a 360 mm TOF tube. S^+ signals were collected by gating the detector so that all ions with a specific mass (and thus specific TOF) were detected. The images were thus 2-D projections of the full 3-D velocity distribution.

Neutral S atoms were ionized using the frequency doubled UV output of a dye laser (Spectra Physics PDL-2) pumped by 532 nm light from an Nd:YAG laser (Quanta-Ray DCR-3). The dye laser operated with rhodamine 6G and DCM dye mixtures, and the UV laser beam was focused ~1 cm away from the molecular beam with a 10 cm focal length lens. The wavelength was set at either 308.2, 309.9, or 311.0 nm in order to provide (2 + 1) resonance enhanced multiphoton ionization (REMPI) of $S(^3P_{2,1,0})$ atoms, respectively, through their $3s^23p^3(^4S°)4p$ $S(^3P)$ state. A typical energy of the tunable UV radiation was 2 mJ per pulse of 5 ns duration.

S atom photoproducts were formed either by dissociation of S_2 by the probe laser beam or by using a separate Nd:YAG and dye laser system in a two-color experiment with different wavelengths for dissociation and ionization. Light with λ = 272−286 nm (line width ~1.0 cm^{-1}) and a typical pulse energy of 1−2 mJ/pulse was produced by frequency doubling (in a KDP crystal) the fundamental output of the dye laser operating with rhodamine 6G and fluorescein dyes. The fourth harmonic of the Nd:YAG laser was used when light of 266 nm wavelength was required. The dissociation laser beam was focused onto or near the molecular beam with a 20 cm focal length lens.

Product S atom detection by (2 + 1) REMPI required a tight laser focus. Detectable levels of signal were only found if the S_2 dissociation laser was also loosely focused to a similar volume. For an allowed one-photon transition, this will lead to some degree of power broadening, especially of the strong B(v′)−X transitions. Experiments were conducted under very similar conditions to our previous study of SH radical photodissociation,[29] for which states of similar lifetime to the predissociating vibrational levels of the B state of S_2 were easily mapped out without undue power broadening by scanning the dissociation laser wavelength. The high power levels may also encourage absorption to a relatively weak continuum, as discussed later.

Two different gas mixtures, 20% OCS or 20% H_2S in Ar, were used to produce S_2. The selected gas mixture passed through the nozzle with a backing pressure of ~1.5 bar, forming a supersonic expansion into the vacuum chamber. The expanding gas pulse passed through an ~ +1000 V open discharge ring located 2 mm downstream from the nozzle. In the OCS/Ar discharge, the background production of S atoms was large, so in the current study, H_2S/Ar mixtures were mainly used. The discharge voltage was set at −1000 V in our previous study of SH photodissociation; in the present work, however, a positive voltage was found to form more S_2 and minimal amounts of SH.

Raw images were Abel inverted using the Gaussian basis sets of the BASEX inversion program[30] to obtain slices through the 3-D velocity distribution. In order to extract information on the $S(^3P_J)$ electronic angular momentum polarization, images were obtained for a variety of pump−probe laser polarization geometries. These involved the regular, linearly polarized laser geometries used to extract alignment parameters of rank K = 2, and labeled HH, VH, and VV according to the polarization of the pump and probe lasers lying parallel (H) or perpendicular (V) to the image plane. In order to correct for detector efficiency, all VH and VV images were point-wise divided by the HH image, which should give a spatially isotropic distribution. Atomic polarizations, evaluated in terms of m_J state population distributions, were calculated using a least-squares fitting method following the formalism of Mo and Suzuki.[31]

Careful calibration to relate radial position in the CCD image to product velocity is an essential component of this study. The factor f for converting ring size in camera pixels to velocity in m/s for VMI[18] is given for our apparatus by $f \sim 1.20\Delta x/\Delta t$, depending slightly on the positions of the laser beams. The most precise calibration was found using one-color $S(^3P_2)$ images, for which the laser operating at the $S(^3P_2)$ REMPI wavelength causes both S_2 dissociation and S atom detection. In these images, rings were observed for all three J states of $S(^3P_J)$ arising from two-photon excitation of S_2, followed by dissociation to the first, second, and third dissociation limits, $S(^3P) + S(^3P)$, $S(^3P) + S(^1D)$, and $S(^3P) + S(^1S)$, respectively. The theoretical total kinetic energy release (TKER) was calculated by TKER = $n\ h\nu - D_0(S_2) - E_{int}$, with n representing the number of photons absorbed, D_0 the bond dissociation energy, and E_{int} the internal energy of the photofragments. The most intense ring in the $S(^3P_2)$ image was the one with the second largest radius, corresponding to the $S(^3P_2) + S(^1D_2)$ channel. The $S(^1D_2)$ copartner has only one E_{int} value, thus a single TKER peak at 20414 cm^{-1}. The kinetic energy of the largest radius ring then matches the calculated value for the $S(^3P_2) + S(^3P_J)$ channel. In this paper, a new value for the S_2 bond energy is reported, but this does not significantly affect the calibration procedure or outcome.

Results

1. Near-Threshold Dissociation: Excitation Wavelengths between 280.5 and 272 nm. Velocity mapped $S(^3P_J)$ images (with J = 2, 1, and 0) from S_2 photodissociation were recorded in the region between 280.5 and 266 nm. A simulated absorption spectrum in this region at 50 K using the constants and linewidths from ref 15, is shown in Figure 2, and exhibits a series of transitions from the vibrational ground state (v″ = 0) of the X state to vibrational levels of the B state with v′ = 10 and above. The onset of predissociation is observed as line broadening within the v′ = 10 band profile, with v′ ≥ 11 bands being diffuse. Raw $S(^3P_2)$ images from the photodissociation of S_2 at different pump laser wavelengths from 280.5 to 272 nm are shown in Figure 3; the wavelengths used are indicated by arrows in Figure 2. The photolysis wavelengths were chosen so that multiphoton excitations resonant with S_2 Rydberg states were avoided. The dissociation limit determined by Ricks and

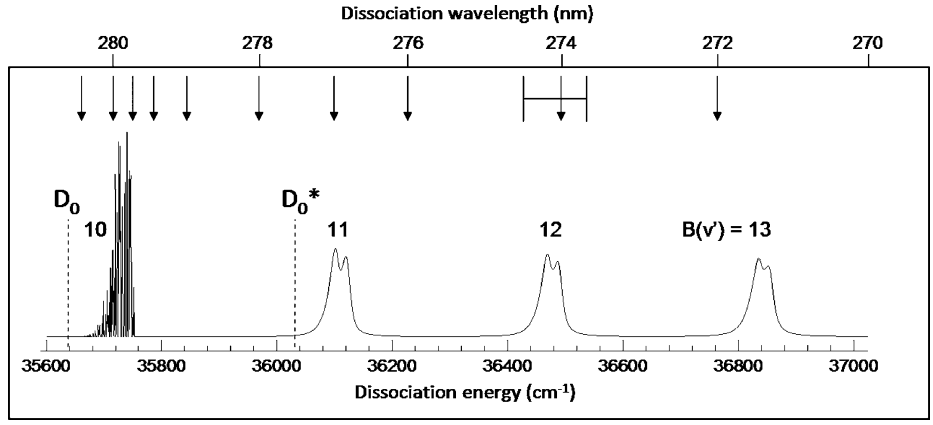

Figure 2. Simulation of the UV absorption spectrum of the B−X transition at a temperature of 50 K from the constants and linewidths given by Wheeler et al.[15] using the PGOPHER program.[32] Velocity map images were obtained for photolysis wavelengths indicated by the position of the vertical arrows. The new value of D_0 obtained in this study is shown by a dashed vertical line, and the second dashed line, labeled by D_0* shows the onset for dissociation to the (2,1) limit.

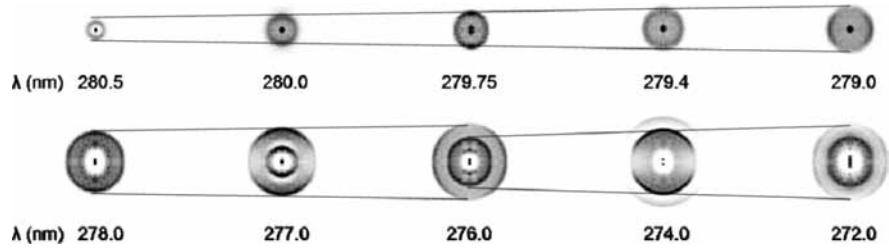

Figure 3. Raw S($^3P_2$) velocity map images from S_2 photodissociation at the indicated wavelengths. The linear photolysis laser polarization is along the vertical axis. Darker regions correspond to higher signal. Straight lines used to connect the same channel in different images are only to help guide the eye, as the energy spacing is irregular.

Barrow,[17] $D_0 = 35240.8$ cm^{-1}, corresponds to a wavelength of 284 nm, but we did not observe any product S atoms until λ was reduced to 280.5 nm. At this threshold wavelength, a ring appeared at the center of the image and grew in size as the wavelength was further reduced from 280.5 to 278 nm. The observed ring only appeared in images obtained for S($^3P_2$) detection in this wavelength range. No rings were found in images for photolysis wavelengths in the same range between 280.5 and 278 nm, but with the probe laser tuned for S($^3P_1$) atom detection. These results indicate that the observed products correspond to the S($^3P_2$) + S($^3P_2$) dissociation limit (the (2,2) limit). Further evidence in support of this assignment is presented in Figure 4, where the kinetic energy distributions for REMPI detection of the three different S(^3P_J) J states are plotted, for the photolysis laser wavelength fixed at 276.0 nm. The spacings of the peaks in the TKER distributions are in good agreement with the known values of the fine-structure splitting for S(^{3}P), confirming the correctness of the velocity calibration factor derived as described in the experimental section.

A plot of the dissociation laser photon energy against the measured peak TKER value for S(^3P_J) atoms should give a straight line with slope 1 and an intercept corresponding to the S_2 dissociation energy. Plots for $J = 2$, 1, and 0 detection are presented in Figure 5; in each case, the cofragment is an S($^3P_2$) atom. From this analysis for the S($^3P_2$) + S($^3P_2$) data (where the slope of the line is indeed 1.0), we determined $D_0 = 35616.1 \pm 8.8$ cm^{-1}; this value is almost 400 cm^{-1} higher than that of Ricks and Barrow for the lowest dissociation limit. From the extrapolation of the same experimental measurements for S($^3P_1$) and S($^3P_0$) (+S($^3P_2$) in both cases), we obtain $D_0 = 35629.5 \pm 4.3$ and 35616.5 ± 9.4 cm^{-1}, respectively. These latter values are less reliable, since fewer wavelengths could be used to excite S_2 above these higher dissociation limits. This difference

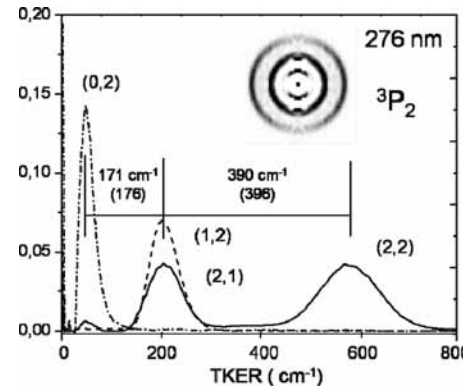

Figure 4. Inverted S($^3P_2$) image (see Figure 3 caption for details) and total kinetic energy release (TKER) distributions for S(^3P_J) atoms, $J =$ 2, 1, 0, from the photodissociation of S_2 at 276 nm. The labels (i, j) indicate S(^3P_i) + S(^3P_j) products, with i referring to the measured atom and j to the cofragment. The solid, dashed, and dash−dot lines are for S(^3P_J) $J = 2$, 1, and 0 detection, respectively. The measured TKER spacing between the peaks at 171 and 390 cm^{-1} agrees well with the known S(^3P_J) $J = 2-1$ and $1-0$ spin−orbit level separations of 176 and 396 cm^{-1}. The (2,2) peak is wider than the (2,1) peak due to the limited pixel resolution of this small image (both rings are one pixel wide at their half-maximum in velocity space, in KER the width increases as velocity squared).

between our D_0 value and the value of ref 17 of ∼400 cm^{-1} matches the spin−orbit splitting between S($^3P_2$) and S($^3P_1$) within the experimental error. The new value for D_0 is, however, consistent with the spectroscopic determinations (Ricks and Barrow, Green and Western) if we reassign the correlation of the dissociative state responsible for the onset of predissociation of the B state to the (2,2) limit, instead of the (2,1) limit, as was argued by Ricks and Barrow. With this revised correlation, the spectroscopic studies would obtain a value for the bond

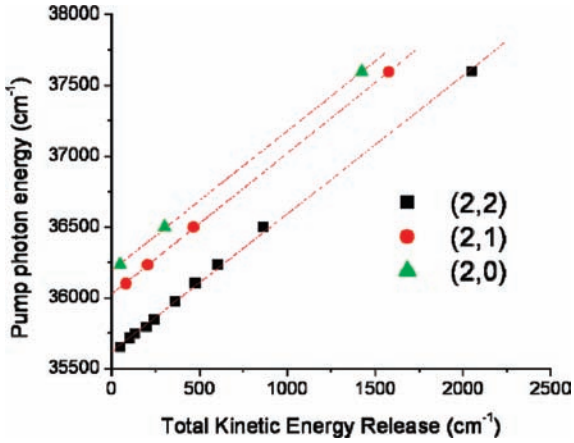

Figure 5. Plots of photolysis laser photon wavenumber against photofragment TKER for $S(^3P_J)$ products of S_2 photodissociation at wavelengths from 266 to 281 nm. Extrapolation to TKER = 0 is used to determine the S_2 bond dissociation energy. Detection of $S(^3P_J)$ with $J = 2$, 1, and 0 is indicated by squares, circles, and triangles, respectively, and the cofragment is $S(^3P_2)$.

dissociation energy to the lowest, (2,2), limit of $D_0 = 35636.9 \pm 2.5$ cm^{-1}, which we report here as the most accurate measure of D_0. The rotational temperature of our molecular beam is estimated to be 30−50 K, which would correspond to average internal energies of 25−45 cm^{-1}, and thus accounts for the small offset between the value determined by VMI and the revised spectroscopic value.

The obtained resolution in kinetic energy release is sufficient to eliminate other possible assignments that could support the old value of D_0. Excitation at 276 nm (36232 cm^{-1}) of $S_2(v=1)$ ($E_{int} = 725$ cm^{-1}), for example, to the old (2,2) limit of 35999.0 cm^{-1} would yield a peak at (36232 + 725 − 35999=) 958 cm^{-1} for (2,2) and at (958 − 396=) = 562 cm^{-1} for (2,1). Although 562 cm^{-1} is close to the 600 cm^{-1} peak in Figure 4, there is no peak around 958 cm^{-1}, and the 600 cm^{-1} peak is shown in Figure 4 to be formed in the (2,2), not the (2,1) channel. Our wide body of data, including shorter wavelength dissociation described below where some signal does arise from vibrationally excited S_2, consistently support the new value of D_0.

2. Dissociation at 269.3 and 266 nm. Two separate types of measurements were carried out at photon energies higher than the near-threshold experiments described above. In the first measurements, S_2 dissociation and $S(^3P)$ ionization were carried out with a single laser tuned to wavelengths around 269.3 nm, which is two-photon-resonant with the S atom $3s^23p^3(^4S°)5p$ $S(^3P)$ state (instead of the 4p ^3P state previously used for $S(^3P)$ REMPI detection). The inverted image and derived TKER distribution for $S(^3P_2)$ detection are shown in Figure 6a. Interference attributed to S^+ production from (2 + 1) REMPI of S_2 via Rydberg states precluded the measurement of similar images for $S(^3P_1)$ and $S(^3P_0)$. In the second set of measurements, the 266 nm fourth harmonic of a Nd:YAG laser was used to dissociate S_2 by means of one-photon absorption; the resulting $S(^3P)$ products were then ionized by the second, probe, laser in a (2 + 1) REMPI process via the $3s^23p^3(^4S°)4p$ $S(^3P)$ state. Resultant images and TKER distributions of the product $S(^3P_J)$ atoms with $J = 2$, 1, and 0 are shown in Figure 6b, c, and d, respectively.

These images were analyzed using the pixel to velocity calibration factor determined above. The TKER values for the various dissociation pathways confirm the revision of the bond dissociation energy discussed in the preceding section. The peaks observed are mainly caused by photodissociation of $S_2(v''=0)$ to the (2,1) limit and $S_2(v''=0,1,2)$ to the (2,2) limit. Dissociation of $S_2(v''=0)$ to the (2,0) channel was not resolved in the $J = 2$ images, but a series of peaks corresponding to photodissociation of $S_2(v''=0-6)$ is observed in the $J = 0$ image at a photolysis wavelength of 266 nm, with an intensity oscillation that is most likely to result from variation in Franck−Condon overlap at the fixed dissociation wavelength. The observation of photodissociation of vibrationally excited S_2 is not surprising when using a discharge source. Production of vibrationally excited species has been reported previously in studies using pulsed electric discharge sources of the type employed in this work; for example, a vibrational temperature of 1700 K was derived for OD production from a D_2O/Ar mixture by Radenović et al.[33]

3. Dissociation at Wavelengths across the B(v′=12)−X Band. For the set of images taken at wavelengths between 280.5 and 266 nm, no significant differences in total signal strength were observed as the dissociation wavelength was varied; i.e., the image intensities were largely independent of whether the photolysis laser wavelength was tuned on- or off-resonance with a B(v′)−X absorption band (Figure 2). The absolute signal strengths are difficult to quantify because of the instability of the discharge source and the high laser powers used. To investigate further the contribution of excitation via the B(v′)−X bands to the photodissociation yields, S_2 was excited at energies from 36430 to 36535 cm^{-1}, in the region of the B(v′=12)−X band. Images were accumulated over 5000 laser shots at 15 cm^{-1} intervals.

The left-hand panel of Figure 7 shows TKER distributions measured at each energy step. Within a factor of ∼50%, the integrated signal from each image (acquired under the same experimental conditions) was found to be constant, independent of the pump laser photon energy. The middle panel shows a simulation of the absorption spectrum for this band at 50 K, as shown in Figure 2.

The right-hand panel of Figure 7 shows photofragment recoil velocity anisotropy (β) parameters derived from fits to the angular dependence of each feature in the velocity map images. For every dissociation wavelength, images with VV, VH, and HH photolysis and probe laser geometries were obtained, and the β-parameter values were extracted using the method of Rose et al.[29] which corrects the angular distributions for the effects of product angular momentum alignment (giving alignment-free β parameters). The $S(^3P_J)$ m_J level population distributions were also obtained from this analysis and are discussed in the next section. Also plotted in the right-hand panel of Figure 7 are values of the β parameter, simulated for the B(v′=12)−X(v″=0) band as a function of excitation energy using the *betaofnu* program of Kim et al.[34] This program does not distinguish the final $S(^3P_J)$ product channels. The simulated β-parameters have positive values because the B−X transition is a parallel, Σ−Σ band, and the variation in β across the band is a consequence of interplay between the excited state lifetime, the rotational period of the excited state (which depends on the rotational angular momentum), and the coherent excitation of P and R branch transitions.[34] The experimental β-parameter values follow some of the predicted variation from the simulations, but with discrepancies that are most pronounced away from the band center where the B−X transition intensity is weaker. The smaller values of β in these regions may indicate a contribution to the absorption from a transition to an excited continuum state via a perpendicular band, or an excitation to a second state with relatively long lifetime (although we would expect such a transition to show additional rotational structure).

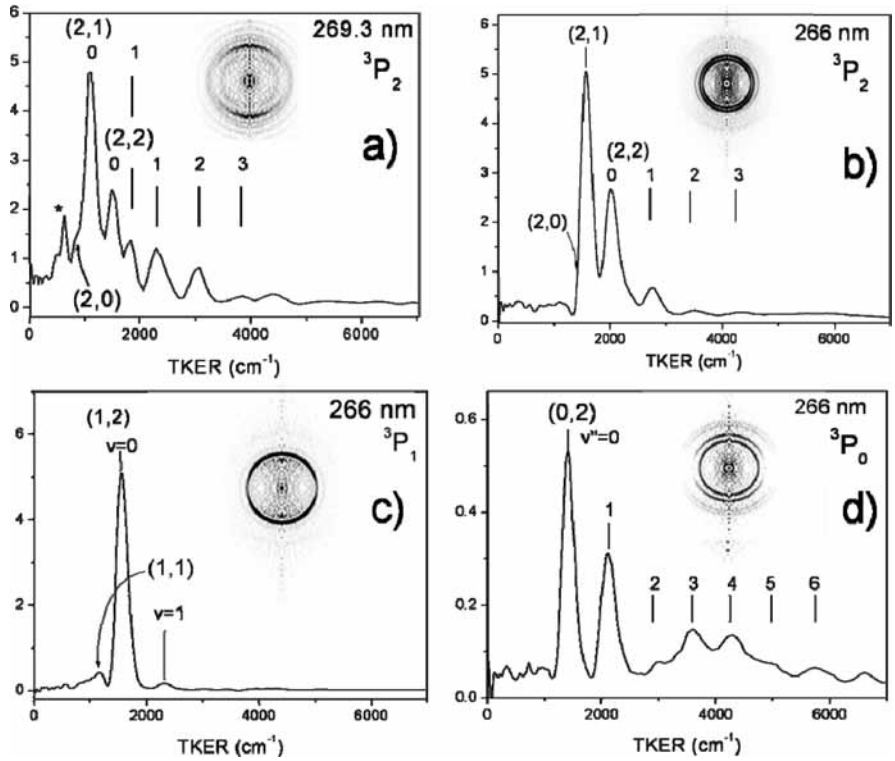

Figure 6. Inverted images and TKER distributions for $S(^3P_J)$ following photodissociation of S_2 at 269.3 and 266 nm. Panels a and b are for $S(^3P_2)$ detection, at respective photodissociation wavelengths of 269.3 and 266 nm; panels c and d show data obtained for $S(^3P_1)$ and $S(^3P_0)$ detection, and a photodissociation wavelength of 266 nm. The vertical lines in the panels indicate features in the TKER distributions that are assigned to photodissociation of $S_2(v'')$ with $v'' = 0$ and above.

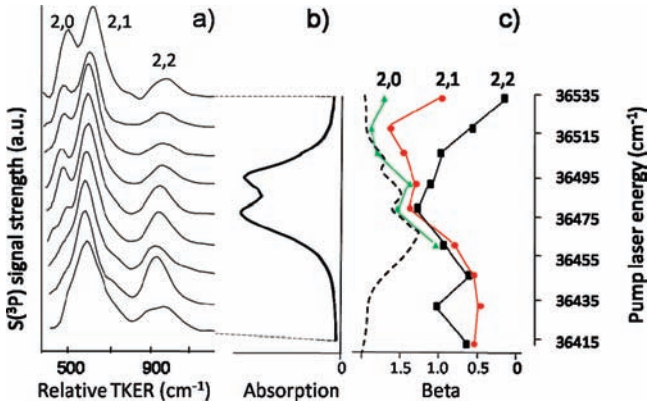

Figure 7. (a) $S(^3P_2)$ atom TKER distributions, (b) simulated S_2 $B(v'=12)$ absorption spectrum at 50 K, and (c) recoil velocity anisotropy parameters, β for S_2 photodissociation in the region from 36415 to 36535 cm^{-1}. The dashed line in the right-hand panel (c) is the result of the betaofnu simulation program[34] (all final channels); see text.

Using the same analysis procedure, alignment-free β parameters for each observed photofragmentation channel were obtained over the much wider wavelength range from 280.5−266 nm, and the results are plotted in Figure 8, along with the position of the $B(v')-X$ transitions. In the vicinity of the threshold for the (2,1) dissociation asymptote, there is a marked change in the β values, suggesting a dominant excitation via a parallel band at shorter wavelengths. To lower energies, the smaller magnitude of β and the indication of negative values suggest, as discussed in the content of the $B(v'=12)-X(v''=0)$ band, an underlying continuum with some perpendicular band character. Oscillations in β are seen in the vicinity of each $B(v')$ band, at $v'=10$ in the (2,2) channel, $v'=11$ in the (2,1) channel, and at $v'=12$ for all channels, as seen in more detail in Figure 7. Thus, while the total yield is found to relatively insensitive

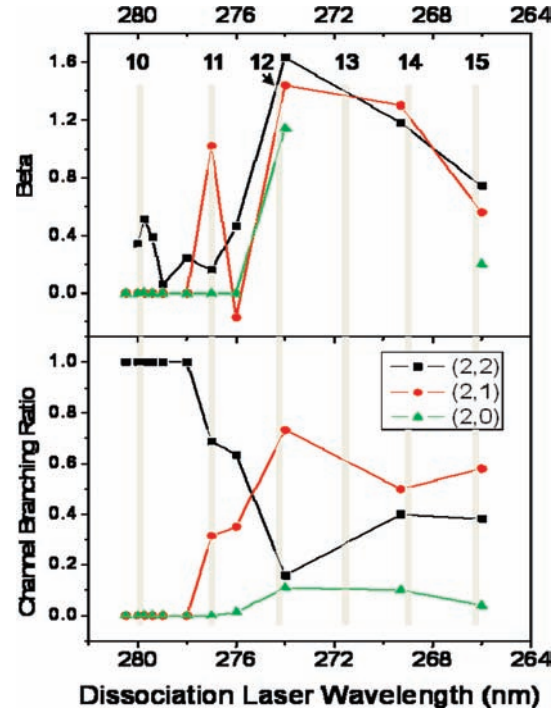

Figure 8. Wavelength dependence of β-parameter values (upper panel) and branching ratios (lower panel) for the (2,2), (2,1), and (2,0) channels. Vertical shaded stripes indicate the positions of the $B(v')$ levels (see Figures 2 and 7). Note that the (2,0) channel β-parameter for 269.3 nm dissociation was not obtainable from the $S(^3P_2)$ image due to overlap (Figure 6a).

to the strong $B(v')$ peaks in the absorption spectrum, the angular distributions for the three channels do appear to be sensitive to resonance with $B(v')$ but in a complex manner.

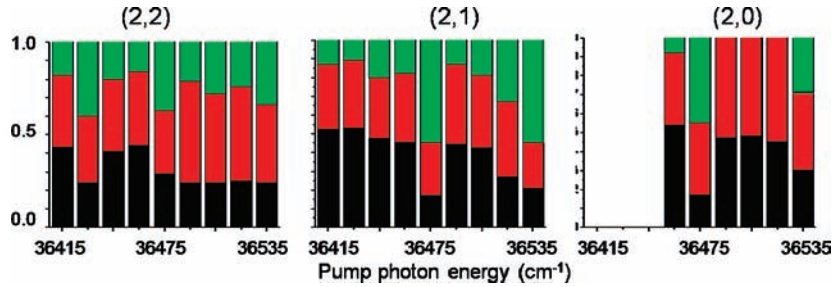

Figure 9. Relative populations of $|m_J|$ levels for the $J = 2$ atoms formed via (2,2), (2,1), and (2,0) photofragmentation channels of S_2: $|m_J| = 2$, green; $|m_J| = 1$, red; $|m_J| = 0$, black. Data are presented at several different dissociation energies that coincide with the region of S_2 absorption in the vicinity of the B(v′=12)−X band.

The lower panel of Figure 8 shows branching ratios into the fine structure components corresponding to the three $S(^3P_J) + S(^3P_2)$ limits. The higher $^3P_1 + {}^3P_1$ and $^3P_1 + {}^3P_0$ limits are energetically accessible at the shorter wavelengths used in this study but were not observed. The $^3P_0 + {}^3P_0$ limit does not give rise to any *u*-symmetry states and is thus not considered further. The measured correlated fine structure distributions show a rapid changeover from exclusively (2,2) products at excitation energies below D_0* (as required on energetic grounds) to preferential population of the (2,1) product states once this threshold is exceeded. This observation is consistent with predissociation of the B state by the $1^1\Pi_u$ state, as modeled by Wheeler et al.[15] Significant population of the (2,2) products remains, however, indicating either another dissociation pathway or nonadiabatic coupling between the $1^1\Pi_u$ state and another, lower-lying dissociative state. A small fraction of the (2,0) product channel is a further indication of nonadiabatic dissociation dynamics.

4. Calculation of m_J Level Population Distributions. Angular distributions obtained in the images for VV, VH, and HH polarization combinations were compared to derive information on electronic angular momentum polarization in the $S(^3P)$ photofragments. Data are presented here for photodissociation at energies across the B(v′=12)−X band; the analysis neglects coherences between m_J state levels and focuses solely on the relative populations. The m_J quantum numbers specify the projection of the electronic angular momentum of the S atoms on the recoil axis. Calculations were performed following the formalism of Mo and Suzuki[31] as implemented by Rose et al.[29] in studies of the photodissociation of SH radicals using the same S atom REMPI detection scheme. The problems associated with the use of this REMPI scheme were discussed in detail by Rose et al.;[29] in particular, the overlapping component transitions of the two-photon excitation step mean that a single $^3P_J \longleftarrow {}^3P_2$ pathway could not be selected. One consequence is that there is an uncertainty in the outcome of the m_J level population calculations because the method of Mo and Suzuki is strictly valid only if there is a change in the *J* quantum number between the initial and final states connected by the two-photon transition. Rose et al.[29] demonstrated that only a small correction is needed for population data derived from analysis of the $^3P_2 \longleftarrow {}^3P_2$ wing of the overlapped absorption feature to match with those obtained from the $^3P_1 \longleftarrow {}^3P_2$ wing of the transition.

The results of the least-squares fitting procedure to the experimental data are presented in Figure 9 for $S(^3P_J)$ detection with an $S(^3P_2)$ cofragment. The general trend is that all three m_J levels are significantly populated, with some marked variations at particular excitation energies, notably at 36475 cm^{-1}, and to a lesser extent at 36535 cm^{-1}.

Discussion

A first general observation for the photodissociation of S_2 is that the yield of $S(^3P)$ atoms is relatively constant across the dissociation continuum, whereas the absorption spectrum shows structure caused by excitation to predissociative levels of the B state, as shown in Figure 2. The lifetimes of these B state levels[15] are typically much shorter than the few-nanosecond time scale for the current measurements of S atom production. The onset of photodissociation to yield exclusively $^3P_2 + {}^3P_2$ S atoms at the lowest energy asymptote is at 35636.9 cm^{-1} above the lowest rotational level of the ground state; a revision of the value of the bond energy is thus indicated, and supported by the TKER measurements for the photofragments. The consequences for interpretation of the S_2 spectrum in the near-threshold region are also discussed below. The $S(^3P)$ yields, and their near-invariance with excitation wavelength, suggest that an important contribution from direct dissociation occurs via excitation to a continuum, but we also note that other signatures of the photodissociation dynamics, such as product recoil angular distributions, branching ratios between competing channels, and m_J level population distributions, show some evidence of dependence on whether the dissociation wavelength is resonant with a B(v′)−X(v″=0) transition of S_2. For example, in Figure 8, the data for the three observed dissociation pathways show clear oscillations in the β-parameter and slow variations in the channel yields, particularly at energies that are nearly resonant with B(v′)−X(v″=0) transitions. In Figure 9, the observed change in the m_J distribution at 36475 cm^{-1} coincides with the absorption peak for the B(v′=12)−X(v″=0) band.

1. D_0 Value and Predissociation of the S_2 B State. The current study demonstrates a need for a revision to the bond energy for S_2. We recommend the value $D_0 = 35636.9 \pm 2.5$ cm^{-1}, taken from the spectroscopic data[17] reinterpreted to be consistent with our TKER-derived value of 35616.1 ± 8.8 cm^{-1}. The spectroscopic value is slightly more precise, and does not have the offset from internal energy of S_2. The reinterpretation requires the predissociation mechanism invoked by Ricks and Barrow to be changed. The earlier work assumed that predissociation of the vibrational levels of the B state at an onset of 35636.9 cm^{-1} is a consequence of crossing to a repulsive $^1\Pi_u$ state correlating with the (2,1) limit; if a different dissociative state is instead involved that correlates to the (2,2) limit, the spectroscopic and photofragment TKER data are brought into quantitative agreement over the value of D_0.

With a revised energy for the limit for dissociation via the (2,1) channel, as indicated by D_0* in Figure 2, the $v' = 10$ level of the B state lies at too low an energy to dissociate to this asymptote. The new value for D_0 thus requires that predissociation from the B(v′=10) level occurs via coupling with the continuum of one or more of the three bound states $A^3\Sigma_u^+$, $c^1\Sigma_u^+$, and $A'^3\Delta_u$ correlating with the lowest $^3P_2 + {}^3P_2$ limit. While such coupling might be expected to be weaker than that involved in a curve crossing, it is nevertheless allowed. The revised interpretation of the energies of the dissociation limits

also provides a satisfactory rationale for several transitions observed by Green and Western in laser induced fluorescence spectra. Two excited states with short (<10 ns) fluorescence lifetimes were identified from transitions at 35723.51 and 35778.18 cm^{-1} from S_2 (X, $v'' = 0$), and there was clear experimental evidence (from double resonance spectra) to associate these excited states with vibrational levels of the B″ electronic state. The original analysis, employing the bond dissociation energy of Ricks and Barrow, placed these two states higher in energy than the $^3P_2 + {}^3P_1$ dissociation limit, which correlation arguments suggest to be the asymptotic dissociation limit of the B″ state. This apparent conflict necessitated a reworking to accommodate a long-range correlation of the $\Omega = 0^+$, 1, and 2 components of the B″ state to the $^3P_2 + {}^3P_0$ asymptote. The revised analysis of the energetics of bond dissociation of S_2 based on our TKER and photodissociation threshold data instead locates the $^3P_2 + {}^3P_1$ limit at 36033.0 cm^{-1}, which is higher in energy than the observed fluorescent vibrational levels of the B″ state. The expected correlation of the B″ state to the $^3P_2 + {}^3P_1$ limit can thus be reinstated. Additional evidence for this revised picture comes from the nature of the fluorescing states seen above the dissociation limit: fluorescence was only observed from very low J levels with $\Omega = 0^+$. The $A^3\Sigma_u^+$, $c^1\Sigma_u^+$, and $A'^3\Delta_u$ states lack $\Omega = 0^+$ components and thus can only cause predissociation of the $\Omega = 0^+$ components of the B″ state by a weak, rotation-induced mixing. The $\Omega = 1$ components of the B″ state, in contrast, can undergo rapid coupling to the continua of one or more of the A, c, and A′ states by a spin−orbit interaction, and thus are too short-lived to be observed in fluorescence. Similarly, very short lifetime fluorescence is observed from B(v'=10) but only for the $\Omega = 0^+$ component.

2. Adiabatic Model for Photodissociation and Nonadiabatic Dissociation Dynamics. Photodissociation of S_2 has been examined here from the $S(^3P_2) + S(^3P_2)$ threshold to nearly 2000 cm^{-1} higher in energy (at $\lambda = 266$ nm). For near-threshold dissociation with relatively heavy, slowly moving fragments, an adiabatic model of the dynamics based on symmetry correlation arguments is first considered. A correlation diagram for dissociation of ungerade electronic states to the spin−orbit resolved levels of the $^3P + {}^3P$ dissociation limit is shown in Figure 10, and is adapted from an equivalent diagram for O_2 given by Huang and Gordon.[35] The m_J level correlations are discussed later.

According to the correlation diagram (and the Wigner−Witmer rules), the $^3P_2 + {}^3P_2$ channel connects with the low-lying bound A, A′, and c states of S_2, which are the analogues of the Herzberg states in O_2. Note that the (2,2) limit is not adiabatically accessible from the B state but can be reached directly by excitation of the continua of the A, A′, and c states. The relatively high yield of the $S(^3P_2) + S(^3P_1)$ channel observed in our photodissociation experiments (Figures 4 and 6) can be explained by predissociation via coupling from the photoexcited state to the $1^1\Pi_u$ state, as was demonstrated in Fermi golden rule (FGR) calculations of predissociation rates for $v' \geq 11$ levels of the B state by Wheeler et al.[15] The $1^1\Pi_u$ state correlates exclusively to the (2,1) atomic limit (Figure 10). As was shown by the FGR calculations, the onset of predissociation by higher-lying repulsive states does not become significant until $v' \geq 17$.

At wavelengths below 276.3 nm, the $^3P_2 + {}^3P_0$ channel becomes energetically accessible, and features observed in the velocity map images are assigned to this channel. As is evident from Figure 10, however, this dissociation limit can only be reached by nonadiabatic coupling; the repulsive $^5\Pi$ state components that correlate to this limit are energetically inaccessible in the Franck−Condon region. The $S(^3P_0)$ image obtained for a dissociation wavelength of 266 nm (Figure 6d) shows significant contributions from vibrationally excited states of S_2 present at low concentrations in the discharge source. Energetically, transitions starting from these higher vibrational levels can still only access the B state or the $1^1\Pi_u$ state, and $S(^3P_0)$ production most likely arises from coupling of dissociative flux on the $1^1\Pi_u$ state to one or more states correlating to the (2,0) limit.

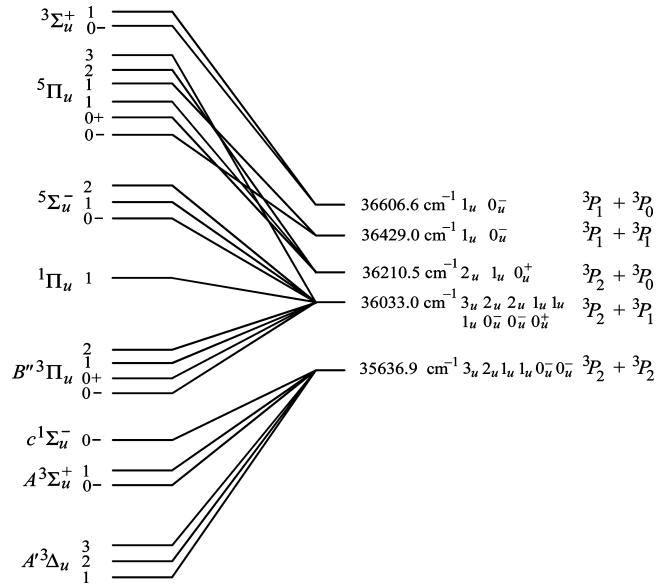

Figure 10. Adiabatic correlation diagram for connecting the u-symmetry electronic states of S_2 to those of the separated $S(^3P)$ atoms. The diagram is redrawn from Green and Western,[14] with changes as discussed in the text. The energy limits are specified with respect to the lowest rotational level of $^{32}S_2$.

In the current study, detailed investigation of the (1,1) and (1,0) product channels was not undertaken, but Figure 6c shows evidence for modest branching into the former channel. As is evident from the correlation diagram shown in Figure 10, these products must also arise from a nonadiabatic dissociation mechanism at the low energies above threshold resulting from the excitation wavelengths used.

3. Direct Dissociation via a Continuum. The near invariance of yields of S atoms with excitation wavelength (e.g., Figure 7) demonstrated by our data indicate that predissociation from the B state is not the sole source of $S(^3P)$ products. Instead, it appears that direct excitation to a continuum provides a significant fraction of the product signal, with the bands displayed in Figure 2 located on top of this unstructured absorption feature. Such an underlying continuum would not have been clearly discernible in the absorption spectroscopy data obtained by CRDS in this wavelength region, nor could continuum absorption have been readily distinguished from light scattering losses by sulfur particulates formed under the flow-discharge conditions used to produce S_2 for these spectroscopic studies. In addition, as discussed in the Experimental Section, the laser powers used for excitation in the current study are relatively high for single photon transitions, so the continuum absorption could be significantly weaker than the B state absorption yet still contribute to our measurements.

Two explanations can be proposed to account for continuum absorption. The first possibility is excitation to the repulsive regions of the bound Herzberg states, above the dissociation limits of these states. As can be seen in Figure 1, reasonable Franck−Condon overlap might be expected between the regions of the repulsive

walls of these potentials and the ground vibrational wave function of S_2. Excitations to all of these Herzberg type states are formally optically forbidden, but transitions can gain intensity by spin−orbit coupling, as was shown for O_2 in previous studies. The intensity borrowing might arguably be more efficient for S_2 than for O_2 because the interacting states are relatively closer in energy and the spin−orbit coupling will be larger. As in O_2, excitation will be encouraged by the high laser power in our experiments ($\sim 10^{20}$ photons/cm^2 at the focal point). Recoil velocity angular distributions for direct dissociation via the Herzberg continuum in O_2 are characterized by $\beta \sim 0.6$ owing to the mixed parallel/perpendicular character of the excitation step. Buijsse et al.[36] reported β values between 0.3 and 0.8 depending on the wavelength and atomic product channel. These observations for O_2 are broadly similar to our findings for velocity map images for S_2 photodissociation obtained at excitation energies below the appearance of the $^3P_2 + {}^3P_1$ channel (see Figure 8). The onset of predissociation of the B state via the $1^1\Pi_u$ state occurs soon after this energy threshold is passed because of the flat nature of the PE curve for this repulsive state for bond lengths from the Franck−Condon region outward. Around this excitation energy region, the β-parameter acquires a positive value that approaches the upper limit of +2 characteristic of a purely parallel transition in a diatomic molecule, consistent with assignment to bands of the $B^3\Sigma_u^- - X\ {}^3\Sigma_g^-$ transition. The continuum excitation could also be borrowing intensity from the optically bright B state.

Van Vroonhoven and Groenenboom carried out a theoretical analysis of direct dissociation of O_2 via the Herzberg continuum and found significant coupling between virtually all states contributing to the Herzberg continuum.[37−39] The interactions might occur through long-range spin−orbit coupling or, for the $A^3\Sigma_u^+$ and the $2^3\Sigma_u^+$ state, radial derivative couplings arising from the kinetic energy operator. Rotationally induced couplings may also play a role but are likely to be weak for the low temperatures of our experiments and thus the low rotational angular momenta of the S_2 molecules. They reported predicted branching ratios for direct dissociation via the different spin−orbit resolved components of the Herzberg states for a semiclassical and an extended diabatic model, that are in reasonably good agreement with the data from Buijsse et al.[36]

The second possible explanation for the continuum absorption in S_2 data invokes excitation to the repulsive wall of the bound $B''^3\Pi_u$ state. While weaker than absorption to the B state, the B″−X transition is electric-dipole allowed, and good Franck−Condon overlap with the S_2 X(v″=0) vibrational wave function is expected in the region of the second dissociation limit. Direct excitation to the B″ continuum should, however, result in recoil velocity angular distributions characterized by $\beta = -1$ (for a perpendicular $\Sigma-\Pi$ transition).

4. m_J Level Populations. The adiabatic correlations presented in Figure 10 can be extended to incorporate analysis of the m_J populations displayed in Figure 9. The adiabatic model for dissociation of the Herzberg states of O_2 was previously developed by van Vroonhoven and Groenenboom, and can be adapted to the case of S_2 dissociation. Briefly, ungerade coupled atomic fine-structure states may be written as

$$|J_a m_a J_b m_b\rangle_u = \frac{1}{\sqrt{2}}[|J_a m_a J_b m_b\rangle - |J_b m_b J_a m_a\rangle] \qquad (1)$$

where $J_a = 2,1,0$ and $J_b = 2,1,0$ are the atomic total angular momentum quantum numbers and m_a and m_b are the projections on the interatomic axis. For a given (J_a, J_b) atomic limit, an ungerade state with a certain Ω quantum number is a linear combination of fine structure states $|J_a m_a J_b m_b\rangle_u$ with $\Omega = m_a + m_b$. The proper linear combination is found by diagonalization of the long-range quadrupole−quadrupole interaction.[37,40] The matrix elements of the interaction operator are given by eq 9 of ref 37 in the molecular basis $|(L)\Lambda S\Sigma\rangle$. Here, Λ, S, and Σ are the usual Hund's case (a) quantum numbers and $L = 0, 1, 2$ is the total orbital angular momentum, which is a good quantum number asymptotically. For ungerade (gerade) states correlating with the $^3P + {}^3P$ limit, $L + S$ is odd (even), and Σ^+ states have even L and Σ^- states have odd L. The assignments of these quantum numbers to all ungerade states that correlate with the $^3P + {}^3P$ limit are given in Table 1 of ref 37. To compute the quadrupole−quadrupole matrix elements in the atomic basis, we transform them to the molecular basis. The transformation matrix elements $\langle J_a m_a J_b m_b | L\Lambda S\Sigma\rangle$ are given by eq 5 in ref 38.

Ungerade states with $\Omega = 0$ and $J_a = J_b$ are odd parity states. For $J_a \neq J_b$, there is one state with $m_a = m_b = 0$, which has parity $(-1)^{J_a+J_b}$, while the other states with $m_a = -m_b$ come in pairs of odd and even parity.

In the analysis below, we consider states that can be reached from the $X^3\Sigma_g^-(0^+)$ and $X^3\Sigma_g^-(1)$ electronic ground states. The allowed parallel transitions to the $B^3\Sigma_u^-(0^+, 1)$ states produce 0_u^+ and 1_u states that can couple to other states of these symmetries through spin−orbit interactions, for which the selection rule is $\Delta\Omega = 0$. Orbit-rotational coupling changes Ω, but we assume this coupling to be relatively unimportant.

The allowed perpendicular transition to the $B''^3\Pi_u$ state can produce 0_u^+, 0_u^-, 1_u, and 2_u states. The forbidden transitions to the Herzberg states involve spin−orbit or orbit−rotational couplings in ground or excited states, resulting in many possible pathways. For oxygen, it is known that the main parallel contribution arises from the $B^3\Sigma_u^-(1) \leftarrow X^3\Sigma_g^-(1)$ transition, followed by spin−orbit coupling to the $A^3\Sigma_u(1)$ state. The perpendicular transitions to the Herzberg states mainly produce 0_u^- and 1_u states.

First, the predictions of the adiabatic model are summarized, and the experimental results are then compared with these predictions. We note that the m_J populations derived in the next sections for the three dissociation limits are in agreement with the wave functions given in Tables 2, 9, and 10 of ref 40.

4a. The $^3P_2 + {}^3P_2$ Limit. For this limit, the asymptotic forms of the ungerade adiabatic states are given in Table 1 of ref 38. The $J = 2$ $|m_J| = 0, 1, 2$ populations p_m derived from these wave functions are presented in Table 1.

TABLE 1: Populations, p_m ($J = 2$), of the $|m_J|$ Levels for the 0_u^- and 1_u States Correlating with the $^3P_2 + {}^3P_2$ Limit for Adiabatic Dissociation

$\lvert m_J\rvert$	$A^3\Sigma_u^+(0^-)$	$c^1\Sigma_u^-(0^-)$	$A'^3\Delta_u(1)$	$A^3\Sigma_u^+(1)$	$A'^3\Delta_u(2)$
0	0	0	0.014	0.486	0.500
1	0.724	0.276	0.500	0.500	0
2	0.276	0.724	0.486	0.014	0.500

4b. The $^3P_2 + {}^3P_1$ Limit. For this limit, we consider one 0_u^+, two 0_u^-, three 1_u, and two 2_u states. The $|m_J|$ level populations are given in Table 2. The 0_u^+ state is lower in energy than the two 0_u^- states when considering the quadrupole−quadrupole interaction.

4c. The $^3P_2 + {}^3P_0$ Limit. For this dissociation limit, as one of the atoms is in a $J_b = 0$ state, there is only one atomic state $|J_a m_a J_b m_b\rangle_u = |2,\Omega,0,0\rangle_u$ corresponding to each adiabatic molecular state with certain Ω. The $\Omega = 0$ state is of even parity (0_u^+), and it correlates with the $|2,0,0,0\rangle_u$ atomic limit, so the adiabatic model predicts $p_0(J=2) = 1.00$. The 1_u state correlates with the $|2,1,0,0\rangle_u$ atomic state, resulting in $p_1(J=2) = 1.00$, and for the 2_u state, we find $p_2(J=2) = 1.00$.

TABLE 2: Populations, p_m ($J = 2$), for the 0_u^+, 0_u^-, 1_u, and 2_u States Correlating with the $^3P_2 + {}^3P_1$ Limit for Adiabatic Dissociation

$\|m_J\|$	$B''^3\Pi_u(0^+)$	$B''^3\Pi_u(0^-)$	$^5\Sigma_u^-(0^-)$	$B''^3\Pi_u(1)$	$^1\Pi_u(1)$
0	0	0.939	0.061	0.082	0.184
1	1.000	0.061	0.939	0.238	0.697
2	0	0	0	0.680	0.119

$\|m_J\|$	$^5\Sigma_u^-(1)$	$B''^3\Pi_u(2)$	$^5\Sigma_u^-(2)$
0	0.734	0	0
1	0.065	1.000	0
2	0.200	0	1.000

4d. Comparison of Experimental Results with the Predictions of the Adiabatic Model. The experimentally derived $|m_J|$ populations shown in Figure 9 for the (2,2) and (2,1) dissociation channels exhibit broadly similar outcomes, with significant population of all three sublevels. As Table 1 illustrates, for the (2,2) limit, this observation is consistent with dissociation via the continua of the A, c, and A′ states, with no single state being dominant. The apparent enhancement in the $|m_J| = 2$ population in the region of excitation of the B(v′=12)−X band could result from predissociation of the $B^3\Sigma_u^-$ state by the c or A′ states. For the (2,1) limit, dissociation via the $B''^3\Pi_u$ and $^1\Pi_u$ states would result in a mixture of populated $|m_J|$ sublevels, as is observed. The greater branching into $|m_J| = 2$ at 36475 cm^{-1} (the vicinity of the B(v′=12)−X band) is suggestive of predissociation of the B state by the $B''(1_u)$ component. The weaker branching to $|m_J| = 2$ sublevels in the (2,0) channel, with concomitant greater population of $|m_J| = 1$ sublevels, is consistent with the above expectations of adiabatic correlation of the 1_u state to this limit (a component of the $^5\Pi_u$ state, accessed, as discussed earlier, by coupling to the $^1\Pi_u$ state), but the observation of significant population of $|m_J| = 0$ sublevels must result from nonadiabatic transitions to the $\Omega = 0^+$ component of the $^5\Pi_u$ state. Likewise, the population of $|m_J| = 2$ sublevels at particular excitation energies implicates nonadiabatic dynamics via the $\Omega = 2$ component of this state. As stated previously, the allowed perpendicular transition to the $B''^3\Pi_u$ state can produce 2_u states.

Conclusions

The photodissociation of diatomic sulfur from its electronic ground state was studied at wavelengths from near threshold at 280.5 to 266 nm using velocity map imaging. Information derived from speed distributions of the $S(^3P_J)$ atomic products demonstrates the need to revise the bond energy of S_2 upward by ∼400 cm^{-1} from previously reported values to 35636.9 ± 2.5 cm^{-1}. The velocity map images also provide mechanistic information on the photodissociation dynamics from determination of photofragment recoil velocity anisotropy parameters and correlated branching into fine-structure components of the two $S(^3P_J)$ atoms. Above the threshold for formation of $S(^3P_2) + S(^3P_1)$ fragments, this becomes the main pathway, but significant fractions of $S(^3P_2) + S(^3P_2)$ products and minor branching to $S(^3P_2) + S(^3P_0)$ products are also observed. Photoproducts corresponding to other fine-structure asymptotes at the $^3P + {}^3P$ limit were not detected (or only very weakly evident) despite being energetically accessible at the shorter wavelengths employed in some of the experiments. The adiabatic correlation of the dissociative $1^1\Pi_u$ state, which crosses (and predisssociates) the bound $B^3\Sigma_u^-$ state, is to the $S(^3P_2) + S(^3P_1)$ asymptote and is thus the likely reason why this channel is favored. Excitation to the $B^3\Sigma_u^-$ state is consistent with the observed recoil anisotropy of the S atoms. The branching to $S(^3P_2) + S(^3P_2)$ and $S(^3P_2) + S(^3P_0)$ channels may be indicative of nonadiabatic dynamics following coupling to the $1^1\Pi_u$ state.

Various pieces of experimental evidence from wavelength dependence of photofragment yields, branching ratios, and anisotropy parameters suggest, however, that there is also an underlying excitation to a continuum that contributes to the formation of S atoms. A mechanism is proposed that involves direct excitation to the repulsive walls of one or more of the bound $A^3\Sigma_u^+$, $A'^3\Delta_u$, or $c^1\Sigma_u^-$ potentials (and perhaps also the continuum of the $B''^3\Pi_u$ state at shorter wavelengths). Excitation to the repulsive walls of the analogous states in O_2 (the Herzberg continuum) is well characterized. The A, A′, and c states dissociate adiabatically to the $S(^3P_2) + S(^3P_2)$ asymptote, and thus may instead be responsible for the branching to this channel

A revised correlation diagram is presented, linking the electronic states of S_2 with the $S(^3P_J) + S(^3P_J)$ asymptotes, with which we draw conclusions about the dissociation mechanisms by interpretation of measured populations of spin−orbit fine-structure levels and m_J sublevels of the $S(^3P_2)$ photofragments. The analysis provides evidence for nonadiabatic dissociation pathways involving several dissociative states.

Acknowledgment. A.J.O.-E. thanks the EPSRC (Programme Grant EP/G00224X) for financial support and the Royal Society and Wolfson Foundation for a Research Merit Award. The work in Nijmegen has been financially supported by the Council for Chemical Sciences of The Netherlands Organization for Scientific Research (CW-NWO).

References and Notes

(1) Spencer, J. R.; Jessup, K. L.; McGrath, M. A.; Ballester, G. E.; Yelle, R. *Science* **2000**, *288*, 1208.
(2) Noll, K. S.; McGrath, M. A.; Trafton, L. M.; Atreya, S. K.; Caldwell, J. J.; Weaver, H. A.; Yelle, R. V.; Barnet, C.; Edgington, S. *Science* **1995**, *267*, 1307.
(3) A'Hearn, M. F.; Feldman, P. D.; Schleicher, D. G. *Astrophys. J. Lett.* **1983**, *274*, L99.
(4) Grim, R. J. A.; Greenberg, J. M. *Astron. Astrophys.* **1987**, *181*, 155.
(5) Kim, S. J.; A'Hearn, M. F.; Larson, S. M. *Icarus* **1990**, *87*, 440.
(6) Liszt, H. S. *Astrophys. J.* **1978**, *219*, 254.
(7) Mitchell, G. F. *Astrophys. J.* **1984**, *287*, 665.
(8) Meyer, K. A.; Crosley, D. R. *Can. J. Phys.* **1973**, *51*, 2119.
(9) Barrow, R. F.; Du Parcq, R. P. In *Elemental Sulfur*; Meyer, B., Ed.; Interscience Publishers: New York, 1965.
(10) Matsumi, Y.; Munakata, T.; Kasuya, T. *J. Chem. Phys.* **1984**, *81*, 1108.
(11) Matsumi, Y.; Suzuki, T.; Munakata, T.; Kasuya, T. *J. Chem. Phys.* **1985**, *83*, 3798.
(12) Pradhan, A. D.; Partridge, H. *Chem. Phys. Lett.* **1996**, *255*, 163.
(13) Green, M. E.; Western, C. M. *J. Chem. Phys.* **1995**, *104*, 848.
(14) Green, M. E.; Western, C. M. *J. Chem. Soc., Faraday Trans.* **1997**, *93*, 365.
(15) Wheeler, M. D.; Newman, S. M.; Orr-Ewing, A. J. *J. Chem. Phys.* **1998**, *108*, 6594.
(16) Berkowitz, J.; Chupka, W. A. *J. Chem. Phys.* **1969**, *50*, 4245.
(17) Ricks, J. M.; Barrow, R. F. *Can. J. Phys.* **1969**, *47*, 2423.
(18) Eppink, A. T; J, B.; Parker, D. H. *Rev. Sci. Instrum.* **1997**, *68*, 3477.
(19) van Brunt, R. J.; Zare, R. N. *J. Chem. Phys.* **1968**, *48*, 4304.
(20) Wigner, E.; Witmer, E. E. *Z. Phys.* **1928**, *51*, 859.
(21) Clark, A. P.; Brouard, M.; Quadrini, F.; Vallance, C. *Phys. Chem. Chem. Phys.* **2006**, *8*, 5591.
(22) Bracker, A. S.; Wouters, E. R.; Suits, A. G.; Lee, Y. T.; Vasyutinskii, O. S. *Phys. Rev. Lett.* **1998**, *80*, 1626.
(23) Parker, D. H. *Acc. Chem. Res.* **2000**, *33*, 563.
(24) Narasimham, N. A.; Apparao, K. V. S. R.; Balasubramanian, T. K. *J. Mol. Spectrosc.* **1976**, *59*, 244.
(25) Chiang, S.-Y.; Lee, Y.-P. *J. Chem. Phys.* **1988**, *89*, 13.
(26) Narasimham, N. A.; Sethuraman, V.; Apparao, K. V. S. R. *J. Mol. Spectrosc.* **1976**, *59*, 142.
(27) Leahy, D. J.; Cyr, D. R.; Osborn, D. L.; Neumark, D. M. *Chem. Phys. Lett.* **1993**, *216*, 503.

(28) Leahy, D. J.; Osborn, D. L.; Cyr, D. R.; Neumark, D. M. *J. Chem. Phys.* **1995**, *103*, 2495.
(29) Rose, R. A.; Orr-Ewing, A. J.; Yang, C.-H.; Vidma, K.; Groenenboom, G. C.; Parker, D. H. *J. Chem. Phys.* **2009**, *130*, 34307.
(30) Dribinski, V.; Ossadtchi, A.; Mandeshtam, V. A.; Reisler, H. *Rev. Sci. Instrum.* **2002**, *73*, 2634.
(31) Mo, Y.; Suzuki, T. *J. Chem. Phys.* **1998**, *109*, 4691.
(32) Western, C. M. *PGOPHER, a Program for Simulating Rotational Structure*; University of Bristol: Bristol, U.K. (http://pgopher.chm.bris.ac.uk). Year of reference is 2007 (version 5.2.343).
(33) Radenovic, D. C.; van Roij, A. J. A.; Chestakov, D. A.; Eppink, A. T. J. B.; ter Meulen, J. J.; Parker, D. H.; van der Loo, M. P. J.; Groenenboom, G. C.; Greenslade, M. E.; Lester, M. I. *J. Chem. Phys.* **2003**, *119*, 9341.
(34) Kim, H.; Dooley, K. S.; North, S. W.; Hall, G. E.; Houston, P. L. *J. Chem. Phys.* **2006**, *125*, 133316.
(35) Huang, Y.-L.; Gordon, R. J. *J. Chem. Phys.* **1991**, *94*, 2640.
(36) Buijsse, B.; van der Zande, W. J.; Eppink, A. T. J. B.; Parker, D. H.; Lewis, B. R.; Gibson, S. T. *J. Chem. Phys.* **1998**, *108*, 7229.
(37) van Vroonhoven, M. C. G. N.; Groenenboom, G. C. *J. Chem. Phys.* **2002**, *116*, 1954.
(38) van Vroonhoven, M. C. G. N.; Groenenboom, G. C. *J. Chem. Phys.* **2002**, *116*, 1965.
(39) van Vroonhoven, M. C. G. N.; Groenenboom, G. C. *J. Chem. Phys.* **2002**, *117*, 5240.
(40) Alexander, A. J. *Phys. Chem. Chem. Phys.* **2005**, *7*, 3693.

JP905104U